



# EUROfusion

EUROFUSION WPJET1-PR(16) 15054

A Shabbir et al.

## **Correlation analysis for energy losses, waiting times and durations of type I edge-localized modes in the Joint European Torus**

Preprint of Paper to be submitted for publication in  
Nuclear Fusion



This work has been carried out within the framework of the EUROfusion Consortium and has received funding from the Euratom research and training programme 2014-2018 under grant agreement No 633053. The views and opinions expressed herein do not necessarily reflect those of the European Commission.

This document is intended for publication in the open literature. It is made available on the clear understanding that it may not be further circulated and extracts or references may not be published prior to publication of the original when applicable, or without the consent of the Publications Officer, EUROfusion Programme Management Unit, Culham Science Centre, Abingdon, Oxon, OX14 3DB, UK or e-mail [Publications.Officer@euro-fusion.org](mailto:Publications.Officer@euro-fusion.org)

Enquiries about Copyright and reproduction should be addressed to the Publications Officer, EUROfusion Programme Management Unit, Culham Science Centre, Abingdon, Oxon, OX14 3DB, UK or e-mail [Publications.Officer@euro-fusion.org](mailto:Publications.Officer@euro-fusion.org)

The contents of this preprint and all other EUROfusion Preprints, Reports and Conference Papers are available to view online free at <http://www.euro-fusionscipub.org>. This site has full search facilities and e-mail alert options. In the JET specific papers the diagrams contained within the PDFs on this site are hyperlinked

---

# Correlation analysis for energy losses, waiting times and durations of type I edge-localized modes in the Joint European Torus

A.Shabbir,<sup>1,2</sup> G.Verdoolaege,<sup>1,3</sup> G.Hornung<sup>1</sup>,O.J.W.F. Kardaun<sup>2</sup>,H.Zohm<sup>2</sup>  
and JET contributors\*

*EUROfusion Consortium, JET, Culham Science Centre, Abingdon, OX14 3DB, UK*

<sup>1</sup>*Department of Applied Physics, Ghent University, B-9000 Ghent, Belgium*

<sup>2</sup>*Max Planck Institute for Plasma Physics, D-85748 Garching, Germany*

<sup>3</sup>*Laboratory for Plasma Physics, Royal Military Academy, B-1000 Brussels, Belgium*

## Abstract

*Several important ELM mitigation techniques are partly motivated by the empirically observed inverse relationship between average ELM energy loss and ELM frequency in a plasma. However, to ensure a reliable effect on the energy released by the ELMs, it is important that this relation is verified for individual ELM events. Therefore, in this work the relation between ELM energy loss ( $W_{ELM}$ ) and waiting time ( $\Delta t_{ELM}$ ) is investigated for individual ELMs in a set of ITER-like wall plasmas in JET. A comparison is made with the results from a set of carbon-wall and nitrogen-seeded ITER-like wall JET plasmas. It is found that the correlation between  $W_{ELM}$  and  $\Delta t_{ELM}$  for individual ELMs varies from moderately positive to zero correlation. Furthermore, most of the unseeded JET ILW plasmas have ELMs that are followed by a second phase referred to as the slow transport event (STE). The effect of the STEs on the distribution of ELM durations is studied, as well as their influence on the correlation between  $W_{ELM}$  and  $\Delta t_{ELM}$ . A high correlation between  $W_{ELM}$  and  $\Delta t_{ELM}$ , comparable to CW plasmas is only found in nitrogen-seeded ILW plasmas. Finally, a regression analysis is performed using plasma engineering parameters as predictors for determining the region of the plasma operational space with a high correlation between  $W_{ELM}$  and  $\Delta t_{ELM}$ .*

## I. INTRODUCTION

Standard high confinement (H-mode) regimes are characterized by the existence of an edge transport barrier (ETB) in a narrow edge region inside the separatrix. Steep pressure gradients in the ETB lead to magnetohydrodynamic (MHD) instabilities called the edge-localized modes (ELMs) [1][2]. ELMs are intense, short duration, repetitive events that cause a partial collapse of the ETB and result in sudden expulsion of energy and particles from the plasma edge. On the one hand, ELMs pose a serious concern as they can cause high transient heat loads on the plasma-facing components (PFCs). On the other hand, they are crucial for regulating the core concentration of impurities, in particular, tungsten (W) which is produced by plasma wall interactions at the divertor target.

---

\*See the Appendix of F. Romanelli et al., Proceedings of the 25th IAEA Fusion Energy Conference 2014, Saint Petersburg, Russia.

31 Given the importance of ELMs for the successful operation of next-step fusion devices, a large  
 32 array of ELM control and mitigation techniques have emerged [3][4]. Typically, ELM losses  
 33 are influenced either, by a complete suppression of the ELMs in regimes where an alternate  
 34 mechanism replaces the energy and particle transport or by increasing the ELM frequency  
 35 ( $f_{ELM}$ ) over its natural value (*ELM pacing*), so that the ELM losses become smaller. The  
 36 effectiveness of the latter method in reducing the peak ELM energy flux ( $q_{max}$ ) at the ITER  
 37 divertor may be dampened in the wake of the experimentally observed linear dependence of the  
 38 effective ELM energy deposition area ( $A_{ELM}$ ) on ELM size ( $W_{ELM}$ ) [5][6][7].

39 However, Loarte *et al.* [8] notes, that while the broadening of  $A_{ELM}$  certainly expands the  
 40 operational regime of uncontrolled ELMs, for conditions in which the uncontrolled ELMs would  
 41 exceed the limits posed by divertor erosion, ELM control will be necessary at ITER. Secondly,  
 42 the processes that lead to the broadening of  $A_{ELM}$  at the divertor will also have a similar effect  
 43 on the scrape-off layer (*SOL*). This will inevitably result in an increase in the energy deposited  
 44 on the ITER's main wall which will consist of Beryllium (*Be*) PFCs. *Be* in contrast to the  
 45 divertor material *W*, has a much lower erosion threshold which makes it highly likely that for  
 46 some conditions the erosion limit of the first wall could constrain uncontrolled ELM operation.

47 Further, the recent ELM pacing experiments at DIII-D using lithium granules in contrast to  
 48 frozen deuterium pellets, report on a reduction of the  $q_{max}$  at the outer strike point [9]. This  
 49 result not only suggests the possibility of reducing  $q_{max}$  at ITER by non-fuel pellet injection  
 50 but also presents an added advantage of de-coupling ELM pacing from plasma fueling.

51 Furthermore, in addition to the protection of PFCs, ELM control requirements at ITER  
 52 have been recently revised to include *W* impurity control [10][8]. Excessive *W* concentration in  
 53 the core can lead to severe central radiation losses which can affect the H-mode performance and  
 54 in extreme cases result in a radiative collapse [11]. Experimental observation at JET [12] and  
 55 AUG [13] have shown that a sufficiently high  $f_{ELM}$  will be required in ITER for maintaining  
 56 an appropriate *W* concentration in the plasma.

57 ELM pacing [14][15], a leading candidate for controlling ( $W_{ELM}$ ) in ITER, relies on the  
 58 observed inverse dependence of  $W_{ELM}$  on  $f_{ELM}$ . For type I ELMs, using a multi-machine  
 59 database and a wide range of plasma parameters averaged over multiple ELM events it has been  
 60 empirically found that [16],

$$\bar{W}_{ELM} = 0.2W_{plasma}\left(\frac{\bar{\Delta}t_{ELM}}{\tau_E}\right). \quad (1)$$

61 Here,  $\tau_E$  is the energy confinement time in plasmas with a stored energy  $W_{plasma}$  and  $\bar{\Delta}t_{ELM}$   
 62 is the average period of the ELM cycle ( $\bar{\Delta}t_{ELM} = 1/f_{ELM}$ ). ELM control methods exploit a  
 63 similar inverse dependence between  $f_{ELM}$  and energy loss by increasing the  $f_{ELM}$  significantly  
 64 beyond the natural frequency, leading to smaller ELM energy losses.

65 As ELM events are repetitive and not periodic,  $\bar{\Delta}t_{ELM}$  is customarily estimated as

$$\bar{\Delta}t_{ELM} = \frac{1}{N} \sum_{i=1}^N \Delta t_{ELM_i}. \quad (2)$$

66 Here  $\Delta t_{ELM_i}$  is the time since the previous ELM and is also frequently referred to as the *waiting*  
 67 *time* of ELM *i*. In this work, in contrast to analyzing the relation of the averages  $\bar{W}_{ELM}$  and  
 68  $\bar{\Delta}t_{ELM}$ , the relation between  $\Delta t_{ELM_i}$  and  $W_{ELM}$  for individual ELMs is investigated in a set

69 of JET plasmas with PFCs made of carbon fiber composites (hereafter carbon-wall or CW)  
70 and ITER material combination (Be and W) (hereafter ITER-like wall or ILW). In an earlier  
71 investigation, Webster *et al.* [17] observed that the inverse dependence between  $W_{ELM}$  and  
72  $f_{ELM}$  is not obeyed by individual ELMs for  $\Delta t_{ELM}$  greater than  $20ms$ . However, their analysis  
73 was restricted to a set of  $2T$ ,  $2MA$  ILW plasmas from the JET tokamak. In this work, the  
74 analyzed plasmas are selected to cover a wide range of plasma parameters in JET. The aim is  
75 to show that an inversely linear relation similar to Equation 1 is obeyed in some plasmas, but  
76 not all. The correlation between  $\Delta t_{ELM}$  and  $W_{ELM}$  is seen to vary in CW discharges and it  
77 is usually low in ILW plasmas, except when nitrogen is seeded into the plasma. This is further  
78 investigated by examining the relation between ELM durations ( $\tau_{ELM}$ ) and  $W_{ELM}$ , as well as  
79 the correlation between energies of consecutive ELMs. This includes a comparative analysis  
80 between ILW and CW plasmas. A weak or no relation between waiting times and ELM energies  
81 could adversely affect the potential of ELM control methods. Therefore, the present work also  
82 aims to emphasize the importance of considering the probability distribution of stochastic plasma  
83 quantities (in this case  $\Delta t_{ELM}$  and  $W_{ELM}$ ), as it contains more information compared to a mere  
84 average.

85 Finally, with the aim to locate regions of the machine operational space where ELM control  
86 would have a reliable effect on ELM energies, a regression analysis is performed of the correlation  
87 between  $\Delta t_{ELM}$  and  $W_{ELM}$  on several global plasma parameters.

88 The structure of the paper is as follows. In section 2, we describe the dataset as well as the  
89 estimation of the ELM characteristics  $\Delta t_{ELM}$ ,  $W_{ELM}$  and  $\tau_{ELM}$ . We also present the statistical  
90 tools that are used to assess the strength of the relation between the various parameters of  
91 interest. In section 3, first the relation between the average quantities is investigated, followed  
92 by a similar analysis on the same quantities for individual ELMs in a specific discharge. We  
93 then study the picture that emerges when all individual ELMs from our database are analyzed  
94 together. This is followed by regression analysis of the correlation between waiting times and  
95 energy losses, as a function of machine parameters in section 4. Finally, in Section 5 we analyze  
96  $W_{ELM}$  of consecutive ELMs before concluding the work in section 6.

## 97 II. DATABASE AND METHODS FOR CORRELATION ANALYSIS

### 98 II.1. Plasma scenario

99 For this investigation, an intermediate size database of 20 CW and 32 ILW JET plasmas has  
100 been compiled. We call this database “JET ELMy database (DBII)”, henceforth referred as JET  
101 ELM-DBII. The dataset has been selected with a view on encompassing a relatively wide range  
102 of plasma and engineering parameters. Each selected discharge has a steady period of H-mode  
103 with regular type I ELMs and the analysis has been restricted to time intervals where plasma  
104 conditions are quasi-stationary. To ensure quasi-stationarity, it has been regarded essential  
105 that in the analyzed time interval the plasmas have approximately constant gas fueling, input  
106 power, edge density and  $\beta_N$ . The size of the current database has somewhat been restricted by  
107 the necessary level of manual intervention for extracting data and in part due to the required  
108 availability of signals with a sufficient temporal resolution. However, the current size of the  
109 database is adequate for the analysis carried out in this work.

		CW	ILW	ILW with $N_2$ seeding
No. of discharges		20	32	6
Toroidal field	$B_t(T)$	1.6 - 3.0	1.3 - 2.7	2.65 - 2.7
Plasma current	$I_p(MA)$	1.5 - 3.0	1.3 - 2.5	2.5
Line-integrated edge density	$n_e(10^{19}m^{-2})$	3.2 - 9.9	1.9 - 7.4	5.4 - 7.4
Input power = $P_{ohmic} + P_{NBI}$	$P_{input}(MW)$	8.1 - 22	6.9 - 19	16 - 19
Main gas ( $D_2$ ) flow rate	$\Gamma_{D_2}(10^{22}s^{-1})$	0.0 - 7.5	0.52 - 4.0	1.3 - 3.7
( $N_2$ ) flow rate	$\Gamma_{N_2}(10^{22}s^{-1})$	-	-	0.76 - 2.8
Average triangularity	$\delta_{avg}$	0.27 - 0.43	0.27 - 0.41	0.27 - 0.39
Edge safety factor	$q_{95}$	2.8 - 3.6	3.1 - 6.1	3.4
Beta normalized	$\beta_N$	1.6 - 2.4	0.92 - 2.0	1.2 - 1.7

Table 1: Range of some key global plasma parameters for the JET ILW, JET CW and the six  $N_2$ -seeded JET ILW plasmas from JET ELM-DBII.

110 With the replacement of CW in JET by the ILW in 2010, it has been observed that the  
111 first wall material appears to have had an effect on both the plasma confinement and pedestal  
112 properties [18][19]. Up until now, the JET-ILW standard baseline scenario has not routinely  
113 achieved a confinement factor of  $H_{98} = 1$  both in low and high triangularity scenarios. The  
114 degraded confinement in JET ILW plasmas is a result of a lower pedestal pressure mainly due  
115 to a pedestal temperature approximately 20-30 percent lower than in JET CW. Pedestal den-  
116 sity on the other hand is comparable among JET CW and JET ILW plasmas. In JET ILW a  
117 pedestal pressure comparable to baseline JET CW has only been achieved in high triangularity  
118 experiments with nitrogen ( $N_2$ ) seeding [19][20]. In the current work, 6 ILW plasmas with  $N_2$   
119 seeding are also included in the dataset, making the total number of analyzed ILW plasmas 38.  
120 The range of a number of important engineering parameters in the database is given in [Table 1](#).  
121

## 122 II.2. ELM detection and energy loss estimation

123 A robust threshold-based algorithm has been developed for estimating ELM temporal properties,  
124 that is  $\Delta t_{ELM}$  and  $\tau_{ELM}$ . The algorithm examines Balmer alpha radiation from Deuterium ( $D_\alpha$ )  
125 for the CW plasmas and Beryllium II (527 nm) radiation for ILW plasmas at JET's inner divertor.  
126 The algorithm uses the sharp spikes in  $D_\alpha$ /Be II radiation for detecting ELMs. This is preceded  
127 by a smoothing process of the time traces and is followed by a threshold-based detection of  
128 ELM start and end times. The estimation of  $\Delta t_{ELM}$  and  $\tau_{ELM}$  is illustrated in [Figure 1](#). The  
129 ELM energy loss has been estimated from the high resolution time-resolved measurement of  
130 the equilibrium stored energy ( $W_{MHD}$ ).  $W_{MHD}$  is calculated by plasma boundary and pressure

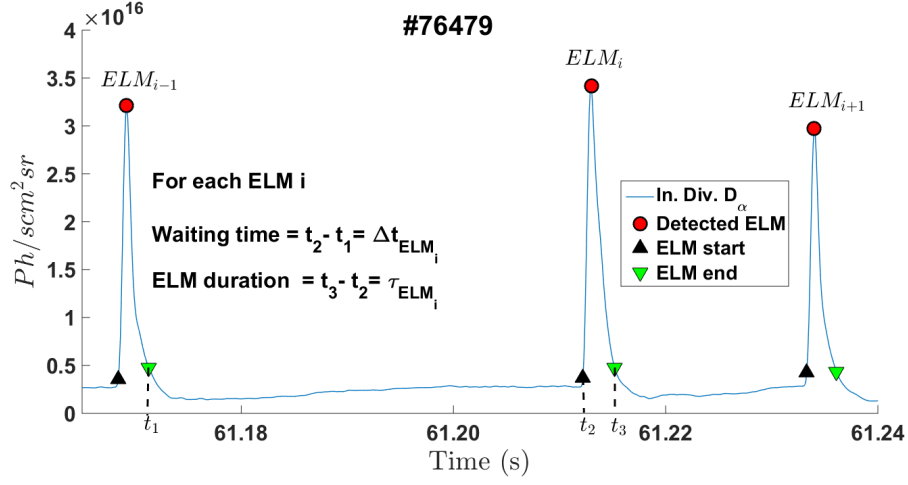


Figure 1: Illustration of the extraction of ELM waiting times ( $\Delta t_{ELM}$ ) and ELM durations ( $\tau_{ELM}$ ) from a time trace of  $D_\alpha$  radiation at JET's inner divertor.

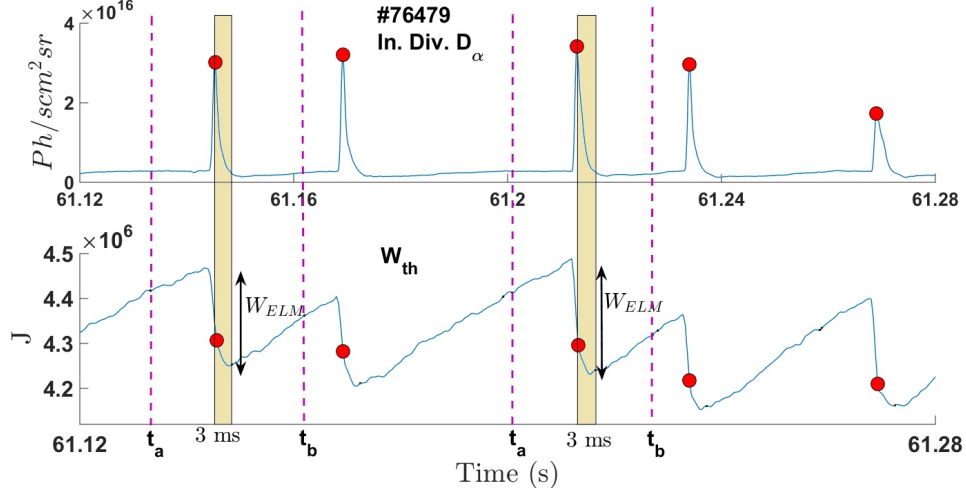


Figure 2: Illustration of ELM energy loss ( $W_{ELM}$ ) estimation from the equilibrium stored energy ( $W_{MHD}$ ), synchronized to the time trace of  $D_\alpha$  radiation at JET's inner divertor.

131 reconstruction, assuming isotropic pressure. The  $W_{MHD}$  time trace is synchronized to individual  
 132 ELMs and  $W_{ELM}$  is estimated as the maximum loss in energy in a small time window around  
 133 an ELM event. This is illustrated in Figure 2. The time window (delimited by  $t_a$  and  $t_b$ ) is  
 134 chosen dynamically, with  $t_a$  taken as 3/4 of the time till the next ELM and  $t_b$  taken as 1/3 of  
 135 the time since the last ELM. Dynamic selection of the time window compensates for the varying  
 136 timescales of ELM energy loss between JET CW and JET ILW plasmas [21]. Further, in order  
 137 to offset inaccuracy arising due to eddy currents in the vacuum vessel and small radial plasma  
 138 motion following an ELM, a time interval of 3 ms has been allowed after an ELM in which the

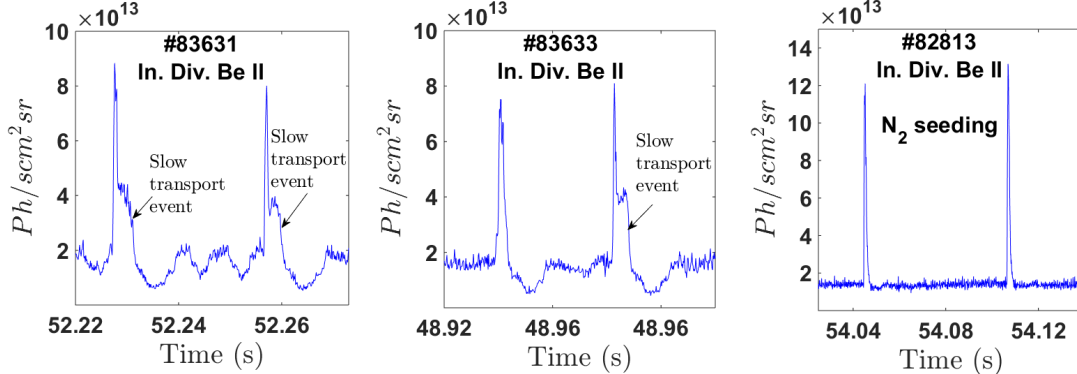


Figure 3: Temporal signature of pure ELMs and ELMs followed by a slow transport event (*STE*) in three typical JET ILW plasmas. The  $N_2$ -seeded plasmas, like CW plasmas, have narrower ELMs and no slow transport events.

139 data is not used for energy loss estimation.

### 140 II.3. ELM duration and slow transport events

141 JET ITER-like wall ELMs are sometimes followed by an extended collapse phase, called the slow  
 142 transport event (STE) [21]. These STEs are analogous to the second phase of ELM collapse  
 143 observed at ASDEX Upgrade (AUG) [20]. The typical temporal signature of an STE is shown  
 144 in Figure 3. ELMs accompanied by an STE have longer time scales of temperature and density  
 145 collapse and result in higher total energy loss of the plasma than the losses produced by ELMs  
 146 alone. We first studied the variation of the energy released by an ELM, averaged over all ELM  
 147 events in a single discharge, in terms of the fraction of STEs. The latter is defined as

$$f_{STE} = \frac{N_{(ELM+STE)}}{N_{ELM} + N_{(ELM+STE)}}, \quad (3)$$

148 where  $N_{(ELM+STE)}$  is the number of ELMs accompanied by a slow transport event and  $N_{ELM}$   
 149 is the number of ELMs that are not followed by an STE phase, hereafter referred to as pure  
 150 ELMs. The ELM energy loss averaged over a single discharge, during stationary conditions, is  
 151 denoted as  $\bar{W}_{ELM}$  and we also consider its ratio w.r.t.  $\bar{W}_{tot}$ , i.e. the total stored equilibrium  
 152 energy in the plasma, also averaged over the entire stationary phase of each discharge that has  
 153 been investigated. The variation of  $\bar{W}_{ELM}$  and  $\bar{W}_{ELM}/\bar{W}_{tot}$  with the fraction of STEs ( $f_{STE}$ )  
 154 for all plasma pulses is plotted in Figure 4. In this work, we have divided JET ILW plasmas ( $N$   
 155 discharges) into three broad categories: those with a high fraction of STEs ( $f_{STE} \geq 50\%$ ,  $N = 4$ ),  
 156 medium fraction of STEs ( $10\% \leq f_{STE} < 50\%$ ,  $N = 24$ ) and those with very few or no STEs  
 157 ( $f_{STE} < 10\%$ ,  $N = 4$ ). From Figure 4, a clear (linear) increase can be noticed of  $\bar{W}_{ELM}$  with  
 158 the fraction of STEs in a plasma. A very similar conclusion is true for the relative energy loss  
 159  $\bar{W}_{ELM}/\bar{W}_{tot}$ , which shows that an increased energy loss is due to a higher fraction of STEs.  
 160 This is in accordance with recent studies wherein it was seen that the STEs carry a significant  
 161 proportion of the energy of the total ELM event [21]. STEs are absent in the JET CW database



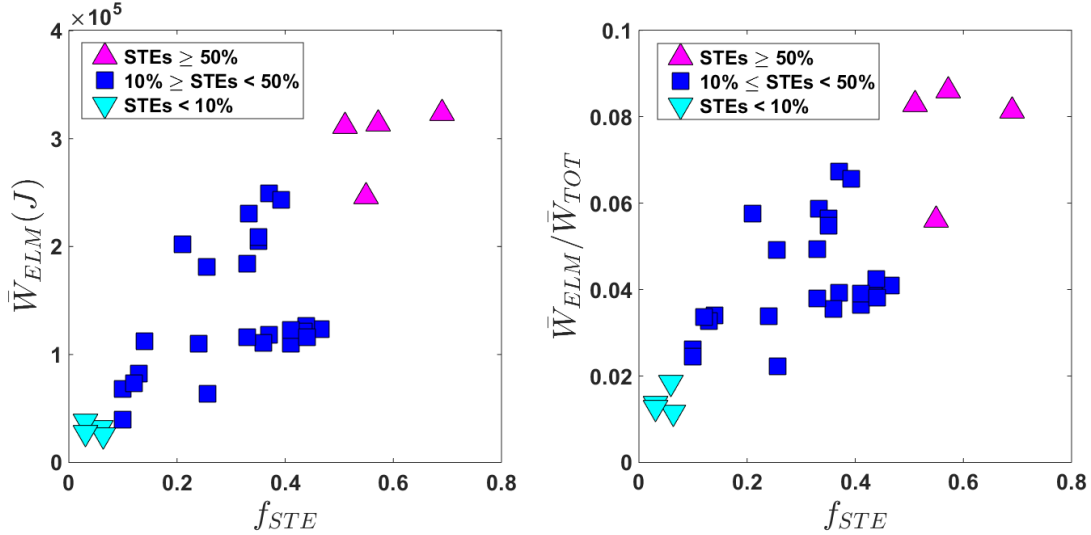


Figure 4: Variation of the mean ELM energy loss ( $\bar{W}_{ELM}$ ) and mean relative ELM energy loss ( $\bar{W}_{ELM}/\bar{W}_{TOT}$ ) with the fraction of slow transport events ( $f_{STE}$ ) in JET ILW plasmas.

162 analyzed in this work. Furthermore, they disappear in  $N_2$ -seeded ILW JET plasmas [21], as  
 163 does the second part of the ELM collapse in AUG plasmas [20]. JET ILW ELMs, compared  
 164 to JET CW plasmas have larger ELM durations ( $\tau_{ELM}$ ). This too, in a large part, is due to  
 165 the existence of STEs in ILW plasmas. The average duration  $\bar{\tau}_{ELM}$  of all ELM events during  
 166 a period of stationary plasma conditions, for the plasmas analyzed in this work, are listed in  
 167 Table 2.  $N_2$ -seeded ILW plasmas and ILW plasmas with low  $f_{STE}$  have  $\bar{\tau}_{ELM}$  similar to CW  
 168 plasmas. ILW plasmas with high  $f_{STE}$  exhibit  $\bar{\tau}_{ELM}$  about three times larger than the  $\bar{\tau}_{ELM}$  of  
 169 CW plasmas. An investigation into the distribution of  $\tau_{ELM}$  yields that the non-seeded JET ILW  
 170 plasmas (high  $f_{STE}$ ) have a distribution of  $\tau_{ELM}$  which is distinctly different from  $N_2$ -seeded  
 171 JET ILW plasmas and JET CW plasmas. The latter two cases exhibit similar distributions for  
 172  $\tau_{ELM}$ . Figure 5 (a)-(c) present the distribution of  $\tau_{ELM}$  for non-seeded JET ILW plasmas (high  
 173  $f_{STE}$ ),  $N_2$ -seeded JET ILW plasmas and JET CW plasmas. The distribution of  $\tau_{ELM}$  for non-

	$\bar{\tau}_{ELM}(ms)$	$std(\tau_{ELM})(ms)$
<b>ILW</b>		
$f_{STE} \geq 50\%$	7.1	3.8
$10\% \leq f_{STE} < 50\%$	3.4	2.2
$f_{STE} < 10\%$	2.7	0.8
$N_2$ -seeded	2.5	0.8
<b>CW</b>	2.6	1.2

Table 2: Typical ELM durations (mean and standard deviation) for unseeded JET ILW plasmas (varying degrees of slow transport events),  $N_2$ -seeded JET ILW plasmas and JET CW plasmas.

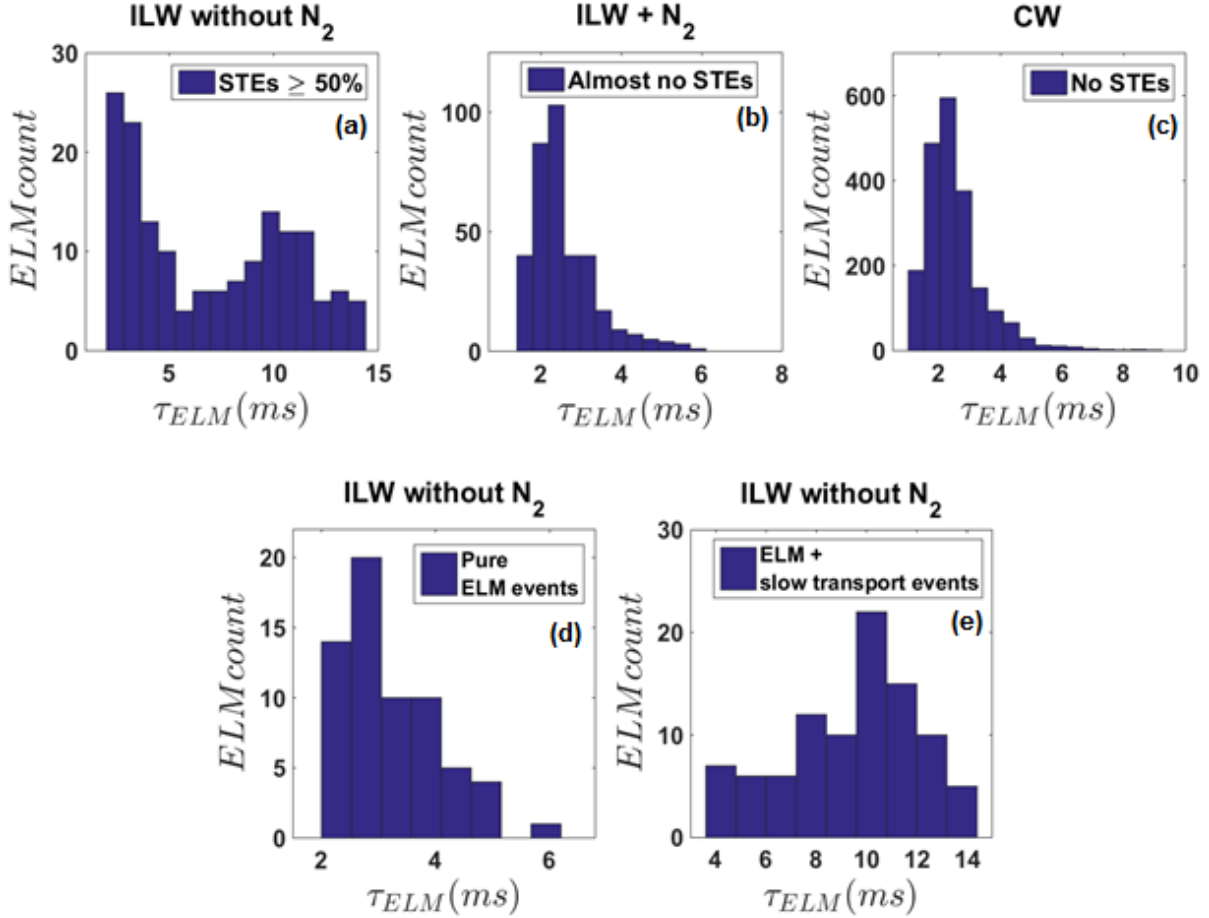


Figure 5: Distribution of ELM durations for various subsets of JET plasmas investigated in this work. In each panel, the vertical axis shows the number of ELM events. (a). Unseeded ILW plasmas with a high  $f_{STE}$ , (b).  $N_2$ -seeded ILW plasmas, (c). CW plasmas, (d). Pure ELMs from high  $f_{STE}$  unseeded ILW plasmas, (e). ELMs followed by  $STEs$  from high  $f_{STE}$  unseeded ILW plasmas.

174 seeded JET ILW plasmas (high  $f_{STE}$ ) is bimodal (two local maxima). The bimodal distribution  
 175 arises as a mixture of two underlying unimodal distributions emerging from collapses due to  
 176 pure ELMs and collapses followed by  $STEs$ . We performed a manual separation of pure ELM  
 177 events from the cases with  $STEs$ , and the corresponding unimodal distributions are shown in  
 178 [Figure 5\(d\)](#) and [\(e\)](#), respectively.

179 The pure ELMs have a duration  $\tau_{ELM}$  that is typically less than about 5 ms, while the ELMs  
 180 with  $STEs$  can last up to 14 ms. The distribution of  $\tau_{ELM}$  for pure ELMs in high  $f_{STE}$   
 181 ILW plasmas ([Figure 5\(d\)](#)) appear similar to the distribution of  $\tau_{ELM}$  for  $N_2$ -seeded JET ILW  
 182 plasmas ([Figure 5\(b\)](#)) and JET CW plasmas ([Figure 5\(c\)](#)). These distributions are visibly non-  
 183 Gaussian with a strong positive skew and we verified that a similar degree of skewness also

JET plasmas		$\bar{\tau}_{ELM}$ (ms)	$std(\tau_{ELM})$ (ms)	$\tilde{\tau}_{ELM}$ (ms)	Skewness
ILW plasmas $f_{STE} \geq 50\%$	Pure ELMs	3.2	0.87	3.0	0.23
	ELMs + STEs	9.6	2.5	9.8	0.08
$N_2$ -seeded ILW plasmas		2.5	0.81	2.3	0.25
CW plasmas		2.6	1.2	2.3	0.25

Table 3: Summary (mean, standard deviation, median and skewness) for the distributions of ELM durations extracted from the JET discharges investigated in this work.

exists in the distribution of ELM durations from individual discharges. From the physical point of view it means that, in our data set, pure ELMs with durations longer than 4 - 5 ms are relatively rare, compared to the prevailing duration of about 2.5 ms. From the statistical point of view, characterization of skewed distributions necessitates additional metrics such as median and mode. The means and standard deviations alongside medians, and skewness estimates for each distribution are summarized in Table 3. Here, the skewness was estimated not from the third-order moment of the distribution (which typically requires a lot of data points), but by dividing the difference between mean and median with standard deviation. For gaining an interesting insight into skewness estimation, the reader may refer to [22]. Contrary to pure ELM events, the distribution of  $\tau_{ELM}$  for ELMs followed by STEs in high  $f_{STE}$  JET ILW plasmas (Figure 5(e)) follow a more symmetric distribution.

#### II.4. Tools for relation analysis

For analyzing the relation between ELM waiting times and energy losses, as a first step we use scatter graphs to get a qualitative impression. Further, in order to quantify the strength of linear relation between  $\Delta t_{ELM}$  and  $W_{ELM}$  for individual ELMs within single discharges, the regular Pearsons product moment correlation coefficient ( $\rho$ ) is estimated [23] [24]. For two sets of data or random variables  $X$  and  $Y$ , this correlation coefficient is defined as

$$\rho_{X,Y} = \frac{cov(X,Y)}{\sigma_X \sigma_Y}, \quad (4)$$

where  $cov$  stands for the covariance between the variables, while  $\sigma_X$  and  $\sigma_Y$  are their standard deviations.  $\rho_{X,Y}$  takes values in the range  $[-1, 1]$ ; a value of 1 means that  $X$  and  $Y$  are perfectly linearly correlated, a value of 0 that there is no correlation, while a value of  $-1$  that they are perfectly anti-correlated.

Further statistical inference that we will perform based on  $\rho$  includes estimation of confidence intervals, testing the significance of correlations and regressing against a set of global engineering parameters. This is complicated by the in general non-Gaussian distribution of a correlation coefficient. Therefore estimates  $r$  of  $\rho$  are converted to a  $z$ -value, which is known to follow an approximately normal distribution:

$$z \equiv \frac{1}{2} \ln \frac{(1+r)}{(1-r)} = \tanh^{-1}(r). \quad (5)$$

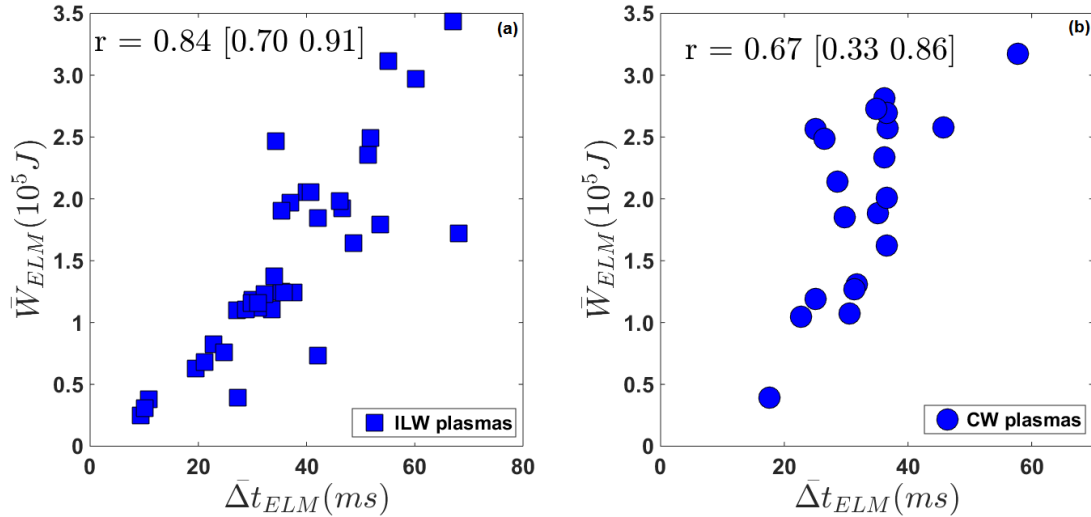


Figure 6: Scatter graphs between  $\bar{W}_{ELM}$  and  $\bar{\Delta}t_{ELM}$  for (a). JET ILW plasmas, (b). JET CW plasmas from JET ELM-DBII. Estimates for the Pearson correlation coefficient ( $r$ ) are indicated, together with the 95% confidence interval.

210 The mean of the distribution is the z-value itself, while the standard deviation does not depend  
 211 on  $r$  and can be approximated by  $\sigma_z = 1/\sqrt{n-1}$ , where  $n$  is the number of data points. In  
 212 addition, we use an alternative measure of relation, in order to capture any possible nonlinear  
 213 relation between the variables under investigation. This is Spearmans rank correlation coefficient  
 214  $r_s$ , which measures monotonic dependence between  $X$  and  $Y$ :

$$r_s = 1 - \frac{6 \sum_{i=1}^n (X_i - Y_i)^2}{n(n^2 - 1)}, \quad (6)$$

215 where,  $X_i$  denotes the rank of the value  $X_i$  in the ordered series of values of the variable  $X$ .  $r_s$   
 216 is a nonparametric measure of dependence and is much less sensitive to outliers. Similar to  $r$ ,  
 217  $r_s$  is in the interval  $[-1,1]$  and  $r_s = 0$  implies no monotonic dependence.

218 Finally, partial correlation is also used when treating ELMs from different plasmas at the  
 219 same time. Partial correlation measures the degree of association between two random variables  
 220 while correcting for the effect of another variable, or several other variables, on this relation.  
 221 The partial correlation of  $X$  and  $Y$ , adjusted for  $Z$  is:

$$\rho_{XYZ} = \frac{\rho_{XY} - \rho_{XZ}\rho_{YZ}}{\sqrt{(1 - \rho_{XZ}^2)(1 - \rho_{YZ}^2)}}. \quad (7)$$

222 Partial correlation can also be computed for Spearmans rank correlation coefficient.

### 223 III. ANALYSIS OF THE RELATION BETWEEN ELM PROPERTIES

224 The relation between  $W_{ELM}$  and  $\Delta t_{ELM}$ , averaged over all ELMs in a single discharge, is shown  
 225 in **Figure 6**(a) and (b) for ILW and CW plasmas, respectively. In agreement with the findings

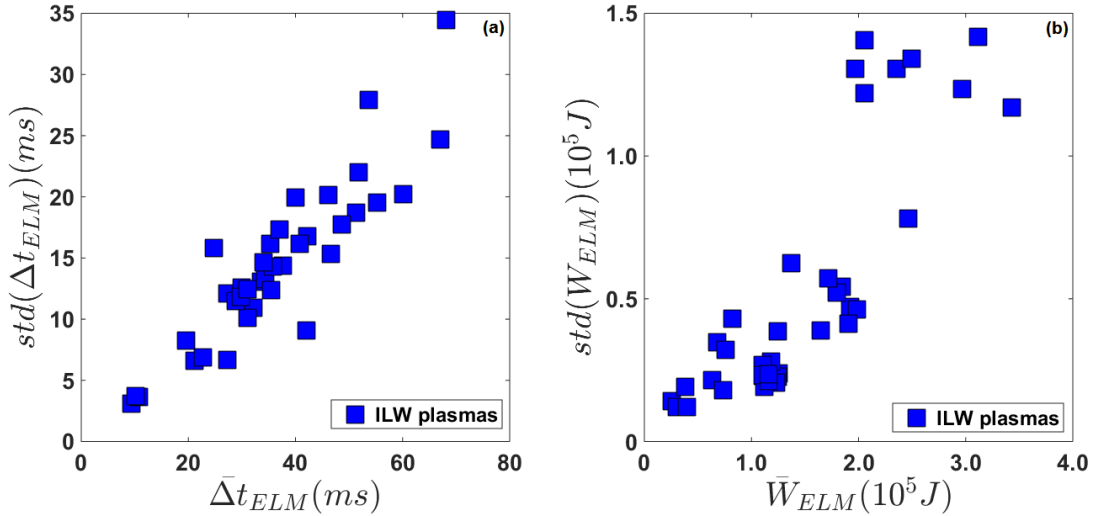


Figure 7: Scatter graphs between mean and standard deviation of (a).  $\Delta t_{ELM}$  and (b).  $W_{ELM}$ , for the JET ILW plasmas.

226 in [16], there is a strongly positive correlation between  $W_{ELM}$  and  $\Delta t_{ELM}$  for ILW plasmas  
 227 as well as for CW plasmas. However, ELM control is targeted at influencing the energy loss  
 228 of individual ELMs. Thus, basing the mitigation strategy on the relation between the average  
 229 properties of different plasmas can possibly be an oversimplification. Furthermore, the relation  
 230 presented in [16] does not take into account the uncertainty on  $W_{ELM}$  and  $\Delta t_{ELM}$ . Nevertheless,  
 231 it can be observed from Figure 7 that the standard deviation of  $W_{ELM}$  and  $\Delta t_{ELM}$  is substantial  
 232 and increases roughly linearly with the mean value. A straightforward extrapolation based on  
 233 Figure 7(b) would suggest 7 - 10 MJ of standard deviation around an absolute  $W_{ELM}$  of 20 -  
 234 30 MJ at ITER.

235 In general, the probability distributions of ELM properties contain comprehensive infor-  
 236 mation about their variability [25][26][27] and therefore studying their statistical correlation  
 237 properties will yield a better insight into the strength of any existing relations. Figure 8 is  
 238 essentially a reproduction of Figure 6, with the addition of the error bars indicating a single  
 239 standard deviation. The strongly linear relations depicted in Figure 6 appears to be less clear  
 240 with the inclusion of standard deviations in Figure 8. Hence, as will be shown below, the effect  
 241 of the spread in  $W_{ELM}$  and  $\Delta t_{ELM}$  within each plasma is better quantified by studying the  
 242 relation between  $W_{ELM}$  and  $\Delta t_{ELM}$  for individual ELMs in a discharge.

243 Furthermore, the relation between  $W_{ELM}$  and  $\tau_{ELM}$  for ILW and CW plasmas is shown in  
 244 Figure 9. The correlation is clearly different in the two cases: ILW plasmas exhibit a strongly  
 245 positive correlation, whereas CW plasmas, failing to reject the null hypothesis of zero correlation  
 246 at 5 percent significance level, effectively show no correlation.

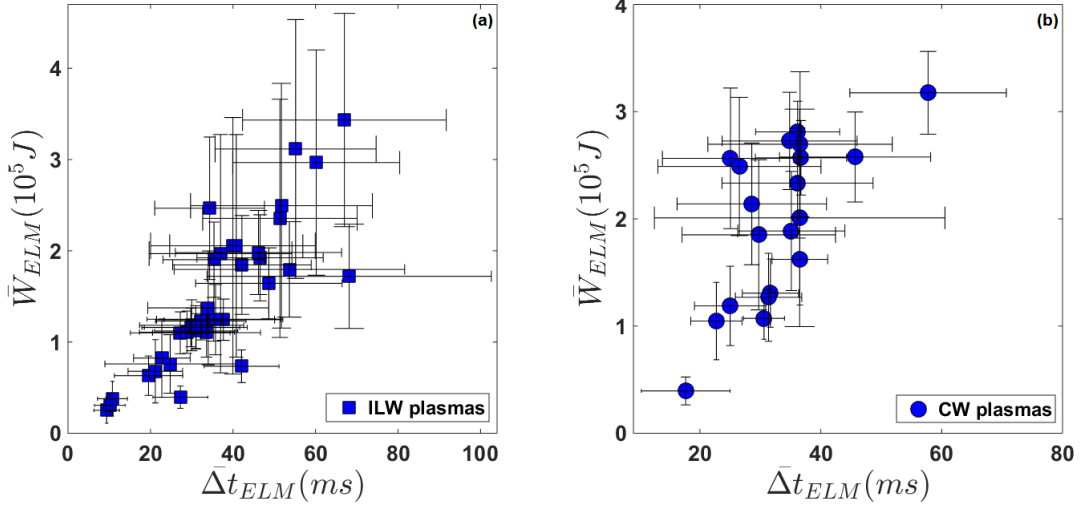


Figure 8: Scatter graphs between  $\bar{W}_{ELM}$  and  $\bar{\Delta}t_{ELM}$ , including the error bars specified by a single standard deviation, for (a). JET ILW plasmas, (b). JET CW plasmas.

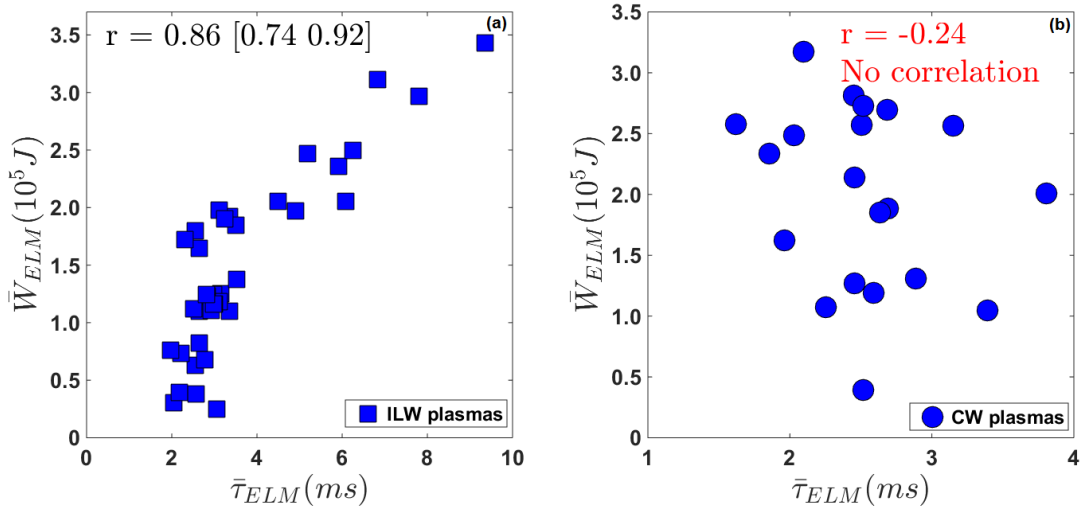


Figure 9: Scatter graphs between  $\bar{W}_{ELM}$  and  $\bar{\tau}_{ELM}$  for (a). JET ILW plasmas, (b). JET CW plasmas. Estimates for the Pearson correlation coefficient ( $r$ ) are indicated, together with the 95% confidence interval. CW plasmas, in contrast to ILW plasmas, fail to reject the null hypothesis of no correlation at 5% significance level.

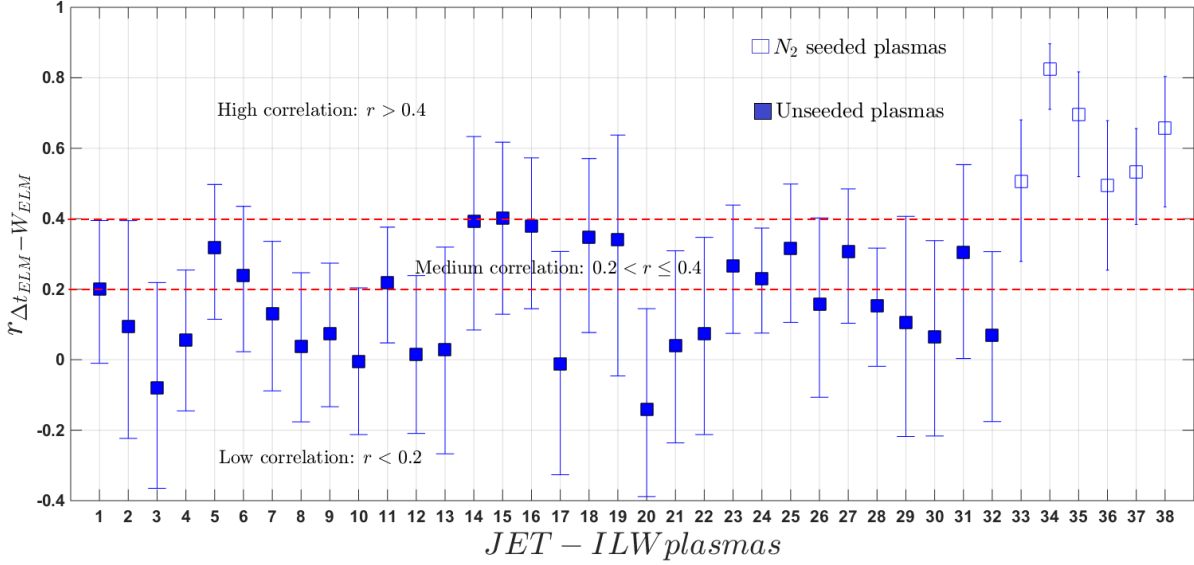


Figure 10: Estimates of linear correlation between  $W_{ELM}$  and  $\Delta t_{ELM}$  for individual ELMs in JET ILW plasmas. 95% confidence intervals are also indicated. Discharges indexed 33 to 38 are  $N_2$ -seeded plasmas.

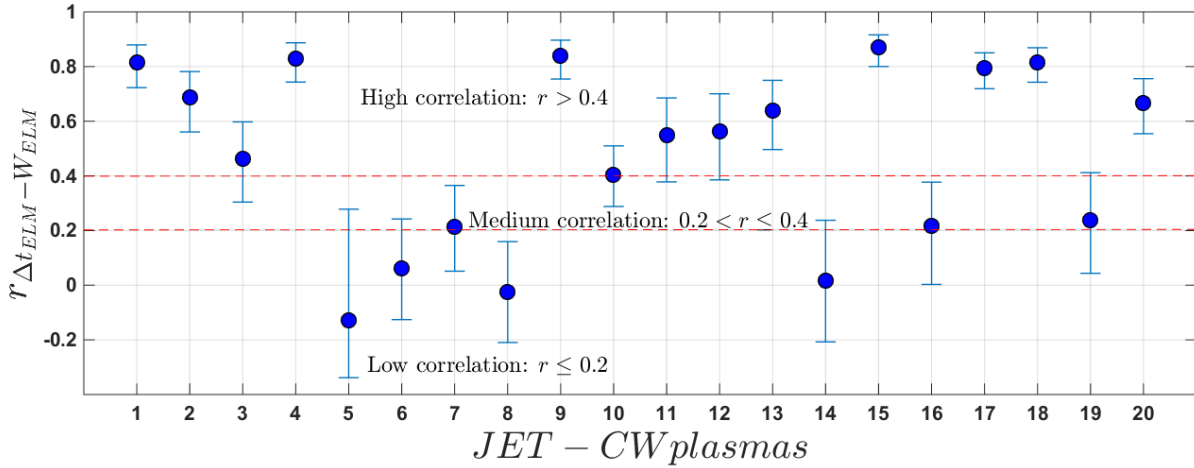


Figure 11: Estimates of linear correlation between  $W_{ELM}$  and  $\tau_{ELM}$  for individual ELMs in JET CW plasmas. 95% confidence intervals are also indicated.

### 247 III.1. Properties of individual ELMs

248 After studying the ELM properties averaged over a window of stationary plasma conditions, we  
 249 now concentrate on relations between the properties of the individual ELMs. Estimates of the  
 250 correlation between  $W_{ELM}$  and  $\Delta t_{ELM}$  ( $r_{\Delta t_{ELM}-W_{ELM}}$ ), along with 95% confidence intervals are  
 251 presented in **Figure 10** and **Figure 11** for individual ELMs in JET ILW and JET CW plasmas,

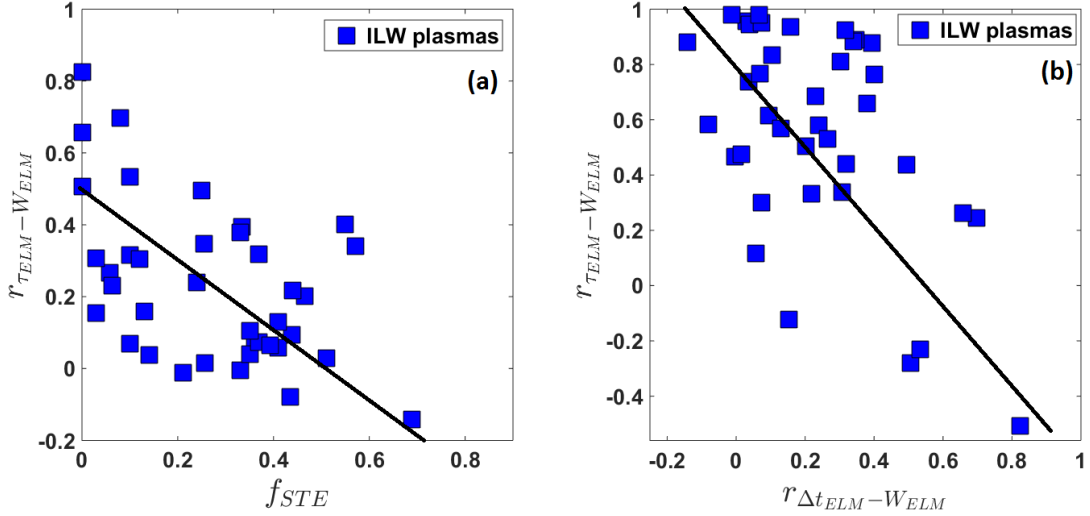


Figure 12: Variation of linear correlation between  $W_{ELM}$  and  $\Delta t_{ELM}$  ( $r_{(\Delta t_{ELM})-W_{ELM}}$ ) for individual ELMs in JET ILW plasmas from JET ELM-DBII, (a). With the fraction of slow transport events ( $f_{STE}$ ), (b). With the linear correlation between  $W_{ELM}$  and  $\tau_{ELM}$  ( $r_{(\tau_{ELM})-W_{ELM}}$ ) for individual ELMs in JET ILW plasmas.

252 respectively. Despite  $W_{ELM}$  and  $\Delta t_{ELM}$  conforming to the expected inverse dependence between  
 253  $W_{ELM}$  and  $f_{ELM}$ , the correlation between  $W_{ELM}$  and  $\Delta t_{ELM}$  for individual ELMs varies from  
 254 being strongly correlated for certain plasmas to being uncorrelated for others. This is observed  
 255 in both CW as well as ILW plasmas. Compared to ILW discharges, CW plasmas on the whole  
 256 have higher correlation between  $W_{ELM}$  and  $\Delta t_{ELM}$  for individual ELMs, with 12 out of the  
 257 20 (60%) analyzed plasmas exhibiting high correlation ( $r > 0.40$ ) and 4 out of the 20 (20%)  
 258 analyzed plasmas demonstrating no correlation ( $r \leq 0.20$ ). On the other hand, out of the 38  
 259 ILW plasmas, only the 6 (16%)  $N_2$ -seeded plasmas exhibit high correlation ( $r > 0.40$ ), whereas  
 260 19 (50%) plasmas show no correlation and 13 (34%) have a medium correlation.

261 The underlying processes causing  $W_{ELM}$  and  $\Delta t_{ELM}$  to exhibit varying degrees of correlation  
 262 could be one or several of the following. The size of  $W_{ELM}$  is controlled by the pedestal  
 263 parameters, i.e. the density and temperature inside the pedestal before the ELM crash [28][29].  
 264 A multi-machine study performed on ASDEX, DIII-D, JT60U and JET CW has established that  
 265 the relative ELM energy losses scale with the inverse of pedestal collisionality [28]. Other key  
 266 parameters that have an important effect on  $W_{ELM}$  are the pedestal width [30], plasma rotation  
 267 [31] and the plasma shape [32]. On the other hand,  $\Delta t_{ELM}$  is a consequence of the various  
 268 timescales involved in the recovery of the pedestal to its pre-ELM state following the ELM  
 269 crash. The pedestal recovery time can be potentially modified by enhanced losses in the inter-  
 270 ELM period, either by increased bulk radiation or by an increased level of density and magnetic  
 271 fluctuations.  $W_{ELM}$ , being determined primarily by the pre-ELM pedestal plasma parameters,  
 272 is likely to remain unaffected by the inter-ELM processes that can potentially modify  $\Delta t_{ELM}$ .  
 273 Furthermore, the peeling-ballooning model, which is a leading candidate for explaining ELM  
 274 onset, fails to explain the phase of saturated gradients without ELMs [33]. In medium-sized



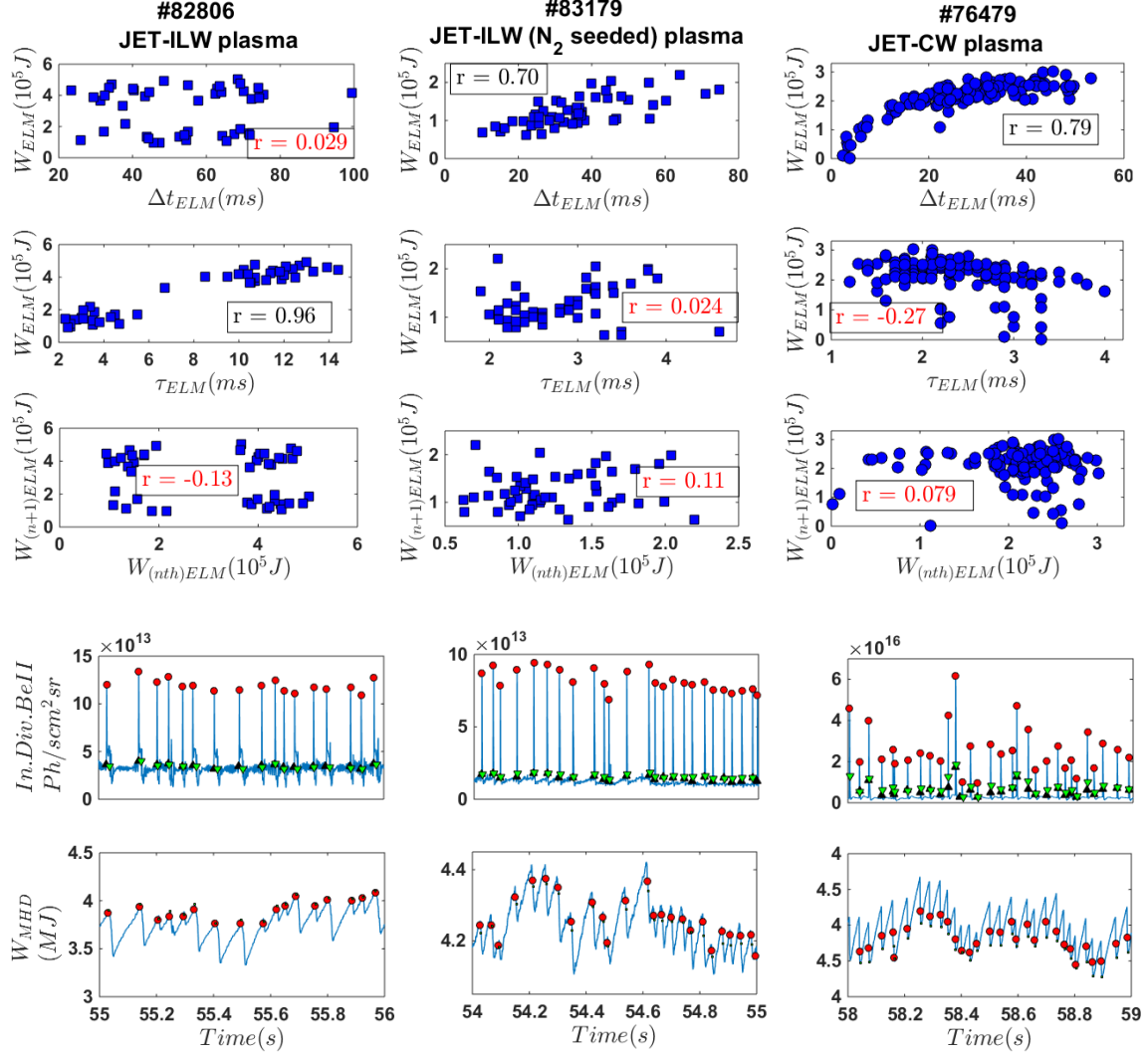


Figure 13: Scatter plot between  $W_{ELM}$  and  $\Delta t_{ELM}$ ,  $W_{ELM}$  and  $\tau_{ELM}$  and  $W_{nthELM}$  and  $W_{(n+1)ELM}$  for JET pulse #82806 (unseeded JET ILW plasma ( $STEs > 50\%$ )), #83179 ( $N_2$ -seeded JET ILW plasma) and #76479 (JET CW plasma). Estimates of  $r$  for each scatter plot are also specified.  $r$  estimates that fail to reject the hypothesis of no correlation at 5% significance level are indicated in color red. Also given are time traces of Be II radiation from the inner divertor (ILW plasmas),  $D_\alpha$  from the inner divertor (CW plasma) and the equilibrium stored energy ( $W_{MHD}$ ).

275 tokamaks at low edge temperature, the bootstrap current seems to be fully developed for a  
 276 relatively long time interval before an ELM crash. It is reasonable to assume that, after the

277 pedestal has recovered, an additional increase in  $\Delta t_{ELM}$  will not lead to an additional increase in  
 278  $W_{ELM}$ . Finally, **Figure 4** suggests that, in the case of the ILW plasmas, the correlation between  
 279  $W_{ELM}$  and  $\Delta t_{ELM}$  for individual ELMs varies inversely with  $f_{STE}$ . Hence, the presence of the  
 280 STEs appears to be at least partly responsible for the observed reduction in correlation between  
 281 ELM waiting times and energies in ILW plasmas.

282 Furthermore, we note that for ILW plasmas there is a weakly inverse relation between the  
 283 correlation among  $W_{ELM}$  and  $\Delta t_{ELM}$  and the correlation among  $\tau_{ELM}$  and  $W_{ELM}$ . It can be  
 284 seen from **Figure 12** that plasmas with high  $f_{STE}$  exhibit no correlation between  $W_{ELM}$  and  
 285  $\Delta t_{ELM}$  and consequently a very high correlation between  $\tau_{ELM}$  and  $W_{ELM}$ . As an illustration,  
 286 scatter plots between  $W_{ELM}$  and  $\Delta t_{ELM}$  and  $W_{ELM}$  and  $\tau_{ELM}$  for three representative plasmas  
 287 are given in **Figure 13**. Non-seeded JET-ILW plasma #82806 with  $f_{STE} \geq 0.5$  exhibits a very  
 288 high correlation between  $W_{ELM}$  and  $\tau_{ELM}$  and no correlation between  $W_{ELM}$  and  $\Delta t_{ELM}$ .  
 289 On the other hand,  $N_2$ -seeded JET-ILW plasma #83179, similar to JET-CW plasma #76479  
 290 demonstrates a high correlation between  $W_{ELM}$  and  $\tau_{ELM}$ .

### 291 III.2. Collective properties of individual ELMs in all analyzed plasmas

292 Next, the collective properties of all ELM events in our JET ILW database are investigated.  
 293 A scatter diagram between  $W_{ELM}$  and  $\Delta t_{ELM}$  for all ELMs (excluding  $N_2$ -seeded plasmas) is  
 294 shown in **Figure 14(a)**. **Table 4** lists the estimates for  $r$  and  $r_s$  corresponding to the scatter  
 295 diagram presented in **Figure 14(a)**. Partial correlations between  $W_{ELM}$  and  $\Delta t_{ELM}$ , while  
 296 controlling for  $B_t$ ,  $I_p$ ,  $P_{input}$ ,  $n_e$ ,  $\Gamma_{D_2}$  and  $\delta_{avg}$ , are presented as well. In this case partial  
 297 correlation is a more realistic measure for assessing the relation between  $W_{ELM}$  and  $\Delta t_{ELM}$ ,  
 298 since it takes into account the widely varying global plasma conditions across the data set. It  
 299 is noteworthy that adjusting for the varied plasma conditions brings a significant reduction in  
 300 the correlation. Moreover, values of  $r_s$  are comparable with  $r$ , which confirms the robustness of  
 301  $r$  estimates.

302 Further, in order to account for any variation of the standard deviation of the data (het-  
 303 eroscedasticity), which is especially clear in **Figure 14(a)** (see also **Figure 7**), a scatter diagram  
 304 between the logarithm of  $W_{ELM}$  and  $\Delta t_{ELM}$  for all ELMs in the analyzed ILW plasmas (exclud-  
 305 ing  $N_2$ -seeded plasmas) is shown in **Figure 14(b)**. Also, on **Figure 14(b)**, the least-squares line  
 306 of best fit is indicated and the corresponding regression coefficients are given in **Table 5**. The  
 307 observed linearity in the log-log space is indicative of a power law relation between  $W_{ELM}$  and  
 308  $\Delta t_{ELM}$ . This implies that the rate of change of  $W_{ELM}$  and  $\Delta t_{ELM}$  decreases gradually up to  
 309 a point beyond which the two quantities become almost independent. This is reaffirmed by the  
 310 inspection of **Figure 14(a)** where there appears to be a saturation of  $W_{ELM}$  for  $\Delta t_{ELM}$  greater  
 311 than 25-30 ms. This is also in agreement with an earlier observation of statistical independence  
 312 between  $W_{ELM}$  with  $\Delta t_{ELM}$  beyond  $\Delta t_{ELM} = 20ms$ , made by Webster *et al.* [17] for individ-  
 313 ual ELMs from a set of  $2T$ ,  $2MA$  JET ILW plasmas. The point beyond which  $W_{ELM}$  becomes  
 314 independent of  $\Delta t_{ELM}$  is likely to be limited by the pedestal recovery time and the total energy  
 315 stored in the plasma. In the plasmas considered in this work, though the plasmas thermal energy  
 316 for pure ELMs appears to increase until the next ELM, it is largely recovered to its pre-ELM  
 317 value in  $25(\pm 8)ms$ . This suggests a scenario in which the edge pedestal is largely restored in  
 318  $\approx 25ms$ , leading to a significant reduction in the correlation between  $W_{ELM}$  for  $\Delta t_{ELM}$  beyond

319  $\Delta t_{ELM} \approx 25ms$ . On the other hand, for ELMs followed by STEs, the plasmas thermal energy  
 320 recovers to its pre-ELM+STE value in  $90(\pm 10)ms$ . It can be seen from [Figure 14\(a\)](#) that ELMs  
 followed by STEs mostly contribute to the cluster of outlier points. Furthermore, it can be

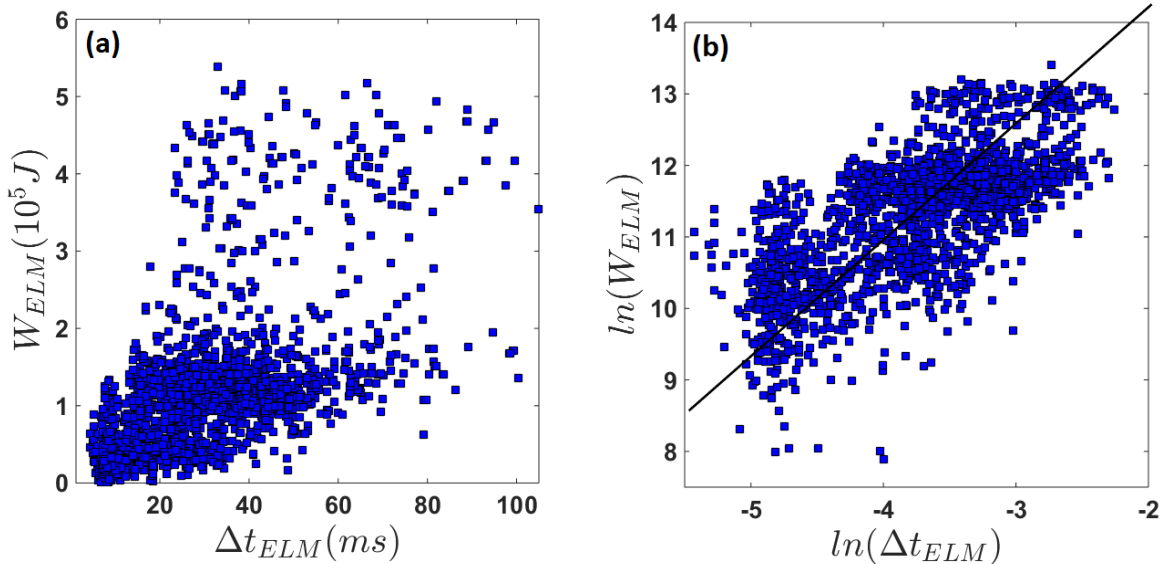


Figure 14: Scatter graph between (a).  $W_{ELM}$  and  $\Delta t_{ELM}$ , (b). Logarithm of  $W_{ELM}$  and  $\Delta t_{ELM}$  for all ELMs in JET ILW plasmas. The least-squares line of best fit to the logarithm of  $W_{ELM}$  and  $\Delta t_{ELM}$  is also shown.

	$r$	$r_s$
<b>Regular</b>	0.58	0.65
<b>Partial</b>	0.21	0.26

Table 4: Estimates of regular and partial correlations, based on Pearson ( $r$ ) and Spearman ( $r_s$ ) coefficients, between  $W_{ELM}$  and  $\Delta t_{ELM}$  for all ELMs in the JET ILW plasmas. The partial correlations control for  $B_t$ ,  $I_p$ ,  $P_{input}$ ,  $n_e$ ,  $\Gamma_{D_2}$  and  $\delta_{avg}$ .

$Model : \ln(W_{ELM}) = \beta_0 + \beta_1 \ln \Delta t_{ELM}$			
$\beta_0$	$\beta_1$	$SE_{\beta_0}$	$SE_{\beta_1}$
14.7	0.895	0.071	0.019

Table 5: Estimated coefficients and standard errors for the least-squares line of best fit shown in [Figure 14\(b\)](#).

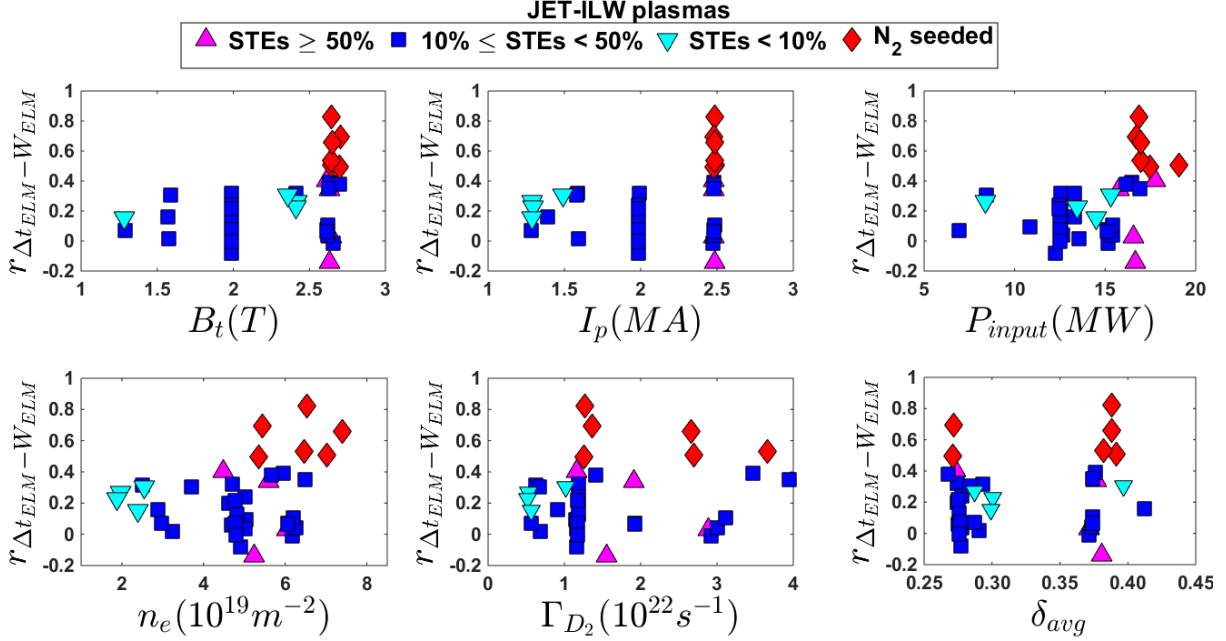


Figure 15: Scatter plots of correlation between  $W_{ELM}$  and  $\Delta t_{ELM}$  ( $r_{(\Delta t_{ELM}-W_{ELM})}$ ) and plasma engineering parameters  $B_t$ ,  $I_p$ ,  $P_{input}$ ,  $n_e$ ,  $\Gamma_{D_2}$  and  $\delta_{avg}$  for JET ILW plasmas.

322 estimated that for ILW ELMs a reduction of  $\Delta t_{ELM}$  from 25-30 ms (beyond which  $W_{ELM}$  and  
323  $\Delta t_{ELM}$  are very weakly correlated) to 10 ms reduces  $W_{ELM}$  by  $\approx 60\%$ . On the other hand, a  
324 reduction of  $\Delta t_{ELM}$  from 50-60 ms to 25-30 ms, reduces  $W_{ELM}$  by  $\approx 40\%$ . This suggests that  
325 if ELMs are consistently paced at 10 ms  $W_{ELM}$  can be reduced by  $\approx 60 - 70\%$ .

#### 326 IV. GLOBAL DEPENDENCE OF CORRELATION BETWEEN ELM ENERGY LOSSES AND 327 WAITING TIMES

328 Since the success of ELM mitigation depends considerably on a high correlation between  $W_{ELM}$   
329 and  $\Delta t_{ELM}$ , we now aim to locate the regions of plasma operational space where the correspond-  
330 ing correlation coefficient  $r_{(\Delta t_{ELM}-W_{ELM})}$  is large. One approach for studying the dependence of  
331  $r_{(\Delta t_{ELM}-W_{ELM})}$  on plasma parameters would be to rely on single parameter scans. In the case  
332 of the present work, there are not enough dedicated experiments available to allow such a study.  
333 Nevertheless, as a preliminary step, in **Figure 15** and **Figure 16** scatter plots between the plasma  
334 engineering parameters  $B_t$ ,  $I_p$ ,  $P_{input}$ ,  $n_e$ ,  $\Gamma_{D_2}$ ,  $\delta_{avg}$  and the correlation coefficient  $r_{(\Delta t_{ELM}-W_{ELM})}$   
335 are provided. It can be observed that in terms of any one plasma parameter, there is no clear  
336 separation between plasmas with a high  $r_{(\Delta t_{ELM}-W_{ELM})}$  and otherwise. As a next step, regres-  
337 sion analysis is used for quantifying the effect of plasma parameters on  $r_{(\Delta t_{ELM}-W_{ELM})}$ . As  
338 discussed in section II.4, the sampling distribution of  $r$  is not normal, therefore  $r$  is transformed  
339 to the quantity  $z$  in (5). Standard multilinear regression using least squares is then performed  
340 for yielding the regression coefficients given in **Table 6**.

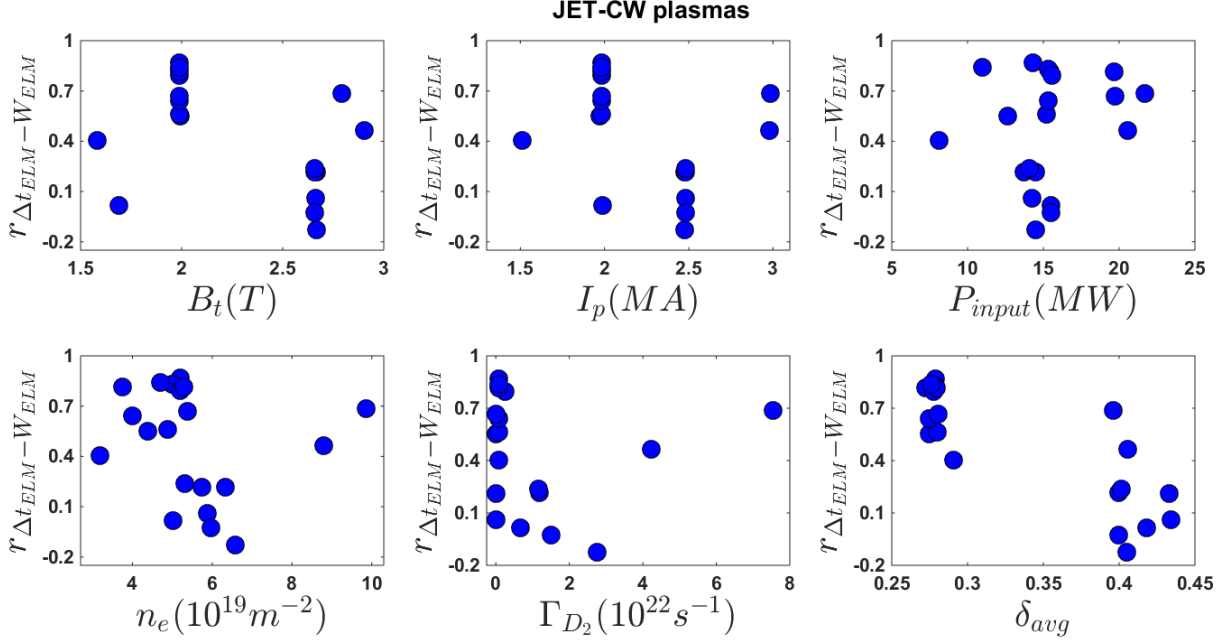


Figure 16: Scatter plots of correlation between  $W_{ELM}$  and  $\Delta t_{ELM}$  ( $r(\Delta t_{ELM} - W_{ELM})$ ) and plasma engineering parameters  $B_t$ ,  $I_p$ ,  $P_{input}$ ,  $n_e$ ,  $\Gamma_{D_2}$  and  $\delta_{avg}$  for JET CW plasmas.

341 The regression model for CW plasmas is constructed using  $B_t$ ,  $I_p$ ,  $P_{input}$ ,  $n_e$ ,  $\Gamma_{D_2}$  and  $\delta_{avg}$   
 342 as predictor variables. For ILW plasmas, however,  $f_{STE}$  is included as an additional predic-  
 343 tor variable, as it has been shown in section III.1 that  $f_{STE}$  has an appreciable influence on  
 344  $r(\Delta t_{ELM} - W_{ELM})$ . In addition, since  $f_{STE}$  is not strictly an engineering quantity, a second model  
 345 (model 2) for ILW plasmas is constructed using  $\Gamma_{N_2}$  as an additional parameter in place of  
 346  $f_{STE}$ . The quality of the fitted regression model is quantified with the root-mean-square error  
 347 (RMSE(%)), which is an indicator of the deviation of the measurements from the model, and  
 348 the coefficient of determination ( $R^2 \in [0, 1]$ ), which measures the degree to which the predictor  
 349 variables and the regression model explain the observed variation of the response variable. Based  
 350 on the values of RMSE and  $R^2$ , each model is fairly appropriate to describe the variation of the  
 351 correlation.

352 Across both model 1 and model 2 that are constructed for ILW plasmas,  $f_{STE}$  or alternatively  
 353  $\Gamma_{N_2}$  appear to be the most important determinant of  $r(\Delta t_{ELM} - W_{ELM})$ . This is expected since  
 354 it has earlier been noted in section III.1 that it is only with  $N_2$  seeding that high values of  
 355  $r(\Delta t_{ELM} - W_{ELM})$  comparable with CW plasmas are obtained. In unseeded ILW plasmas the  
 356 correlation fluctuates at most to a weakly positive correlation from a state of no correlation.  
 357 Secondary to  $f_{STE}/\Gamma_{N_2}$ ,  $\delta_{avg}$  and  $\Gamma_{D_2}$  are the more important determinants of  $r(\Delta t_{ELM} - W_{ELM})$ .  
 358 This is consistent with the model for CW plasmas as therein  $\delta_{avg}$  followed by  $\Gamma_{D_2}$  appear as the  
 359 most important of the considered plasma engineering parameters. It is important to note that  
 360 in addition to the global time-averaged plasma engineering parameters, the regression models  
 361 could substantially benefit if the complete distributions of the predictor parameters would be

	CW	ILW	
		Model 1	Model 2
C	1.67 [0.43 2.92]	-0.457 [-1.1 0.15]	0.029 [-0.56 0.62]
$B_t(T)$	-0.982 [-2.4 0.41]	0.0483 [-0.30 0.39]	0.162 [-0.14 0.46]
$I_p(MA)$	1.62 [-0.66 3.9]	0.559 [-0.43 1.5]	0.0791 [-0.69 0.85]
$P_{input}(MW)$	-0.0229 [-0.089 0.043]	0.0119 [-0.036 0.060]	0.0080 [-0.038 0.054]
$n_e(10^{19}m^{-2})$	0.165 [-0.11 0.44]	-0.0259 [-0.24 0.19]	-0.0486 [-0.25 0.15]
$\Gamma_{D_2}(10^{22}s^{-1})$	<b>-0.113</b> [-0.26 0.039]	<b>-0.114</b> [-0.24 0.012]	<b>-0.0422</b> [-0.17 0.084]
$\delta_{avg}$	<b>-8.54</b> [-12 -5.4]	<b>-0.313</b> [-2.2 1.5]	<b>-0.618</b> [-2.3 1.1]
$f_{STE}$	–	<b>-1.19</b> [-1.7 -0.65]	–
$\Gamma_{N_2}(10^{22}s^{-1})$	–	–	<b>0.269</b> [0.16 0.38]
RMSE(%)	23.4	18.3	17.4
$R^2$	0.83	0.64	0.67

Table 6: Least-squares multilinear regression fits (including a cut-off term C) for correlation between  $W_{ELM}$  and  $\Delta t_{ELM}$  using global plasma parameters as predictors. The coefficient estimate alongside 95% confidence intervals are presented, together with the root-mean-square error (RMSE) and the coefficient of determination ( $R^2$ ).

362 considered.

## 363 V. RELATION BETWEEN ENERGY LOSS OF SUCCESSIVE ELMs

364 Finally, the relationship between energy losses of consecutive ELMs is investigated. As can be  
365 noted from [Table 7](#), only 10 - 15 percent of the analyzed JET-ILW (including  $N_2$ -seeded plasmas)  
366 and JET-CW plasmas exhibit a weak non-zero correlation. Also, the values of  $r_s$  are in agreement  
367 with estimates of  $r$ .  $W_{ELM}$  of consecutive ELMs is largely uncorrelated. This implies that an  
368 ELM with a large  $W_{ELM}$  is equally likely to be followed by an ELM with a large or small  $W_{ELM}$ .  
369 Further, this observation is consistent across unseeded JET-ILW plasmas,  $N_2$ -seeded JET-ILW  
370 plasmas and JET-CW plasmas. This can also be observed in the scatter plots of  $W_{ELM}$  of  $n$ th  
371 ELM and  $W_{ELM}$  of  $(n + 1)$ th ELM in [Figure 13](#). For each of the three representative plasmas,  
372 #82806, #83179 and #76479,  $W_{ELM}$  of successive ELMs is uncorrelated.

## 373 VI. CONCLUSIONS

374 This work examines the relation between  $W_{ELM}$  and  $\Delta t_{ELM}$  for individual ELMs in a set  
375 of non-seeded JET-ILW plasmas and compares the results with a set of  $N_2$ -seeded JET-ILW  
376 plasmas and JET-CW plasmas. It is found that the empirically established inverse relation  
377 between average  $f_{ELM}$  and  $\bar{W}_{ELM}$  is not ubiquitously obeyed by individual ELMs. The linear  
378 correlation between  $W_{ELM}$  and  $\Delta t_{ELM}$  varies from being strongly correlated for certain plasmas  
379 to being completely uncorrelated for others. CW plasmas, in general, exhibit higher correlation

Plasmas	$-0.3 < r \leq 0.1$	$0.1 < r \leq 0.3$	$r > 0.3$	$r \neq 0$ ( $\alpha = 5\%$ )	$r \neq 0$ ( $\alpha = 1\%$ )
ILW	20	15	3	4	2
CW	16	4	0	3	0

Table 7: Number of ILW plasmas (including  $N_2$ -seeded plasmas) and CW plasmas with correlation between energy loss of successive ELMs  $r > 0.3$ ,  $0.1 < r \leq 0.3$  and  $-0.3 < r \leq 0.1$ . The number of plasmas with  $r$  significantly different from zero are also indicated at two significance levels  $\alpha$ .

380 between  $W_{ELM}$  and  $\Delta t_{ELM}$  than ILW plasmas and it is only in  $N_2$ -seeded ILW plasmas that a  
381 high correlation comparable to certain CW plasmas is observed.

382 Further, ELMs in non-seeded JET ILW plasmas are often followed by a slow transport  
383 event resulting in a bi-modal distribution of ELM durations. The two modes correspond to two  
384 distinct underlying phenomena: pure ELMs and ELMs followed by a slow transport event. Slow  
385 transport events are not present in JET-CW plasmas and they disappear in  $N_2$ -seeded JET-ILW  
386 plasmas, giving rise to a unimodal asymmetric distribution of ELM durations. The average ELM  
387 energy loss in a plasma scales linearly with the proportion of ELMs followed by slow transport  
388 events in a plasma, whereas the linear correlation between  $W_{ELM}$  and  $\Delta t_{ELM}$  varies inversely  
389 with the fraction of slow transport events. Further, JET-ILW plasmas demonstrate a weakly  
390 inverse relation between the linear correlation of  $W_{ELM}$  and  $\Delta t_{ELM}$  and the linear correlation  
391 between  $\tau_{ELM}$  and  $W_{ELM}$ . It is noteworthy that  $\bar{W}_{ELM}$  and  $\bar{\tau}_{ELM}$  appear to be uncorrelated  
392 in JET-CW plasmas but possess a strongly positive correlation in JET-ILW plasmas.

393 A collective analysis of all the ELMs from the unseeded JET-ILW ELMs plasmas revealed  
394 that the variation between  $W_{ELM}$  and  $\Delta t_{ELM}$  obeys a power law relationship.  $W_{ELM}$  appears  
395 to saturate for  $\Delta t_{ELM} \approx 25 - 30ms$  which is roughly the time taken for the plasma thermal  
396 energy to return to its pre-ELM value. This suggests a scenario where the linear correlation  
397 between  $W_{ELM}$  and  $\Delta t_{ELM}$  significantly reduces as the edge pedestal recovers to its pre-ELM  
398 value.

399 Further, least squares linear regression is employed for determining the region of the plasma  
400 operating regime where the correlation between  $W_{ELM}$  and  $\Delta t_{ELM}$  is maximized A regression  
401 model is constructed using plasma and engineering parameters for both JET-ILW and JET-CW  
402 plasmas. While the models will certainly benefit from more informative predictors, they never-  
403 theless indicate the more important parameters from the plasma parameters used as predictors.  
404 For the JET-ILW plasmas,  $\Gamma_{N_2}$  followed by  $\delta_{avg}$  and  $\Gamma_{D_2}$  contribute most to the correlation  
405 between  $W_{ELM}$  and  $\Delta t_{ELM}$ . Similarly, for JET-CW plasmas  $\delta_{avg}$  and  $\Gamma_{D_2}$  appear to be the  
406 most important determinants of correlation.

407 Lastly it is acknowledged that  $W_{ELM}$  and  $\Delta t_{ELM}$  are stochastic quantities and a precise  
408 analysis of these quantities needs to effectively incorporate the uncertainty on these quantities. It  
409 has also been shown that the standard deviation of  $W_{ELM}$  and  $\Delta t_{ELM}$  increases linearly with the  
410 mean value. Analyzing  $W_{ELM}$  and  $\Delta t_{ELM}$  for individual ELMs subtly allows for the standard  
411 deviation in  $W_{ELM}$  and  $\Delta t_{ELM}$  to be accommodated and indeed reveals additional information.

412 It is emphasized that analyzing complete probability distributions of  $W_{ELM}$ ,  $\Delta t_{ELM}$ ,  $\tau_{ELM}$  and  
413 other plasma parameters will yield a more comprehensive picture and will thus form the basis  
414 of future investigations.

415

#### ACKNOWLEDGEMENT

416 This work has been carried out within the framework of the EUROfusion Consortium and has  
417 received funding from the EURATOM research and training programme 2014-2018 under grant  
418 agreement No 633053. The views and opinions expressed herein do not necessarily reflect those  
419 of the European Commission. The authors would like to thank Lorenzo Frassinetti for his useful  
420 feedback on this work.

421

#### REFERENCES

- 422 [1] H. Zohm, “Edge localized modes (ELMs),” *Plasma Physics and Controlled Fusion*, vol. 38,  
423 no. 2, pp. 105–128, 1996.
- 424 [2] J. Wesson, *Tokamaks*, 4th ed. Oxford University Press, 2011.
- 425 [3] P. Lang, A. Loarte, G. Saibene, L. Baylor, M. Becoulet, M. Cavinato, S. Clement-Lorenzo,  
426 E. Daly, T. Evans, M. Fenstermacher, Y. Gribov, L. Horton, C. Lowry, Y. Martin,  
427 O. Neubauer, N. Oyama, M. Schaffer, D. Stork, W. Suttrop, P. Thomas, M. Tran, H. Wil-  
428 son, A. Kavin, and O. Schmitz, “ELM control strategies and tools: status and potential for  
429 ITER,” *Nuclear Fusion*, vol. 53, no. 4, p. 043004, 2013.
- 430 [4] T. Evans, “ELM mitigation techniques,” *Journal of Nuclear Materials*, vol. 438, pp. S11–  
431 S18, 2013.
- 432 [5] T. Eich, H. Thomsen, W. Fundamenski, G. Arnoux, S. Brezinsek, S. Devaux, A. Herrmann,  
433 S. Jachmich, J. Rapp, and J.-E. contributors, “Type-I ELM power deposition profile width  
434 and temporal shape in JET,” in *Journal of Nuclear Materials*, vol. 415, no. 1 SUPPL, 2011.
- 435 [6] M. W. Jakubowski, T. E. Evans, M. E. Fenstermacher, M. Groth, C. J. Lasnier, A. W.  
436 Leonard, O. Schmitz, J. G. Watkins, T. Eich, W. Fundamenski, R. A. Moyer, R. C. Wolf,  
437 L. B. Baylor, J. A. Boedo, K. H. Burrell, H. Frerichs, J. S. DeGrassie, P. Gohil, I. Joseph,  
438 S. Mordijck, M. Lehnen, C. C. Petty, R. I. Pinsker, D. Reiter, T. L. Rhodes, U. Samm,  
439 M. J. Schaffer, P. B. Snyder, H. Stoschus, T. Osborne, B. Unterberg, E. Unterberg, and  
440 W. P. West, “Overview of the results on divertor heat loads in RMP controlled H-mode  
441 plasmas on DIII-D,” *Nuclear Fusion*, vol. 49, no. 9, p. 14, 2009.
- 442 [7] H. Thomsen, T. Eich, S. Devaux, G. Arnoux, S. Brezinsek, E. DelaLuna, W. Fundamenski,  
443 A. Herrmann, A. Huber, S. Jachmich, P. Lomas, I. Nunes, G. Saibene, A. Scarabosio,  
444 J. Schweinzer, and J.-E. contributors, “Power load characterization for type-I ELMy H-  
445 modes in JET,” *Nuclear Fusion*, vol. 51, no. 12, p. 123001, 2011.



- 446 [8] A. Loarte, G. Huijsmans, S. Futatani, L. Baylor, T. Evans, D. M. Orlov, O. Schmitz,  
447 M. Becoulet, P. Cahyna, Y. Gribov, A. Kavin, A. S. Naik, D. Campbell, T. Casper, E. Daly,  
448 H. Frerichs, A. Kischner, R. Laengner, S. Lisgo, R. Pitts, G. Saibene, and A. Wingen,  
449 “Progress on the application of ELM control schemes to ITER scenarios from the non-  
450 active phase to DT operation,” *Nuclear Fusion*, vol. 54, no. 3, p. 033007, 2014.
- 451 [9] A. Bortolon, R. Maingi, D. K. Mansfield, A. Nagy, A. L. Roquemore, L. R. Baylor, N. Com-  
452 maux, G. L. Jackson, E. P. Gilson, R. Lunsford, P. B. Parks, C. Chrystal, B. A. Grierson,  
453 R. Groebner, S. Haskey, M. J. Makowski, C. J. Lasnier, R. Nazikian, T. Osborne, D. Shi-  
454 raki, and M. A. V. Zeeland, “High frequency pacing of edge localized modes by injection of  
455 lithium granules in DIII-D H-mode discharges,” *Nuclear Fusion*, vol. 56, no. 056008, 2016.
- 456 [10] E. de la Luna, I. Chapman, F. Rimini, P. Lomas, G. Saibene, F. Koechl, R. Sartori,  
457 S. Saarelma, R. Albanese, J. Flanagan, F. Maviglia, V. Parail, A. Sips, E. Solano, and  
458 J. contributors, “Understanding the physics of ELM pacing via vertical kicks in JET in  
459 view of ITER,” *Nuclear Fusion*, vol. 56, no. 2, p. 026001, 2016.
- 460 [11] A. Kallenbach, R. Neu, R. Dux, H.-U. Fahrbach, J. Fuchs, L. Giannone, O. Gruber, A. Her-  
461 mann, P. Lang, B. Lipschultz, C. Maggi, J. Neuhauser, V. Philipps, T. Puetterich, V. Ro-  
462 hde, J. Roth, G. Sergienko, A. Sips, and ASDEX Upgrade Team, “Tokamak operation with  
463 high-Z plasma facing components,” *Plasma Physics and Controlled Fusion*, vol. 47, no. 12B,  
464 2005.
- 465 [12] R. Neu, G. Arnoux, M. Beurskens, V. Bobkov, S. Brezinsek, J. Bucalossi, G. Calabro,  
466 C. Challis, J. W. Coenen, E. De La Luna, P. C. De Vries, R. Dux, L. Frassinetti, C. Giroud,  
467 M. Groth, J. Hobirk, E. Joffrin, P. Lang, M. Lehnen, E. Lerche, T. Loarer, P. Lomas,  
468 G. Maddison, C. Maggi, G. Matthews, S. Marsen, M. L. Mayoral, A. Meigs, P. Mertens,  
469 I. Nunes, V. Philipps, T. Pütterich, F. Rimini, M. Sertoli, B. Sieglin, A. C. C. Sips, D. Van  
470 Eester, G. Van Rooij, and J.-E. contributors, “First operation with the JET International  
471 Thermonuclear Experimental Reactor-like wall,” *Physics of Plasmas*, vol. 20, no. 5, 2013.
- 472 [13] R. Dux, A. Janzer, T. Puetterich, and ASDEX Upgrade Team, “Main chamber sources  
473 and edge transport of tungsten in H-mode plasmas at ASDEX Upgrade,” *Nuclear Fusion*,  
474 vol. 51, no. 5, p. 119501, 2011.
- 475 [14] P. Lang, J. Neuhauser, L. Horton, T. Eich, L. Fattorini, J. Fuchs, O. Gehre, A. Herrmann,  
476 P. Ignácz, M. Jakobi, S. Kálvin, M. Kaufmann, G. Kocsis, B. Kurzan, C. Maggi, M. Manso,  
477 M. Maraschek, V. Mertens, A. Mück, H. Murmann, R. Neu, I. Nunes, D. Reich, M. Reich,  
478 S. Saarelma, W. Sandmann, J. Stober, U. Vogl, and the ASDEX Upgrade Team, “ELM  
479 frequency control by continuous small pellet injection in ASDEX Upgrade,” *Nuclear Fusion*,  
480 vol. 43, no. 10, pp. 1110–1120, 2003.
- 481 [15] Y. Liang, “Overview of Edge Localized Modes Control in Tokamak Plasmas,” *Fusion Sci-*  
482 *ence and Technology*, vol. 59, no. 3, pp. 586–601, 2011.
- 483 [16] A. Herrmann, “Overview on stationary and transient divertor heat loads,” *Plasma Physics*  
484 *and Controlled Fusion*, vol. 44, no. 6, pp. 883–903, 2002.

- 485 [17] A. J. Webster, S. J. Webster, and J.-E. contributors, “Processes and properties of edge-  
486 localised instabilities in 2T 2MA plasmas in the Joint European Torus,” *Physics of Plasmas*,  
487 vol. 21, no. 11, p. 112502, 2014.
- 488 [18] M. Beurskens, L. Frassinetti, C. Challis, C. Giroud, S. Saarelma, B. Alper, C. Angioni,  
489 P. Bilkova, C. Bourdelle, S. Brezinsek, P. Buratti, G. Calabro, T. Eich, J. Flanagan,  
490 E. Giovannozzi, M. Groth, J. Hobirk, E. Joffrin, M. Leyland, P. Lomas, E. de la Luna,  
491 M. Kempenaars, G. Maddison, C. Maggi, P. Mantica, M. Maslov, G. Matthews, M.-L.  
492 Mayoral, R. Neu, I. Nunes, T. Osborne, F. Rimini, R. Scannell, E. Solano, P. Snyder,  
493 I. Voitsekhovitch, and P. de Vries, “Global and pedestal confinement in JET with a Be/W  
494 metallic wall,” *Nuclear Fusion*, vol. 54, no. 4, p. 043001, 2014.
- 495 [19] C. Giroud, G. Maddison, S. Jachmich, F. Rimini, M. Beurskens, I. Balboa, S. Brezin-  
496 sek, R. Coelho, J. Coenen, L. Frassinetti, E. Joffrin, M. Oberkofler, M. Lehnen, Y. Liu,  
497 S. Marsen, K. McCormick, A. Meigs, R. Neu, B. Sieglin, G. van Rooij, G. Arnoux, P. Belo,  
498 M. Brix, M. Clever, I. Coffey, S. Devaux, D. Douai, T. Eich, J. Flanagan, S. Grünhagen,  
499 A. Huber, M. Kempenaars, U. Kruezi, K. Lawson, P. Lomas, C. Lowry, I. Nunes, A. Sirin-  
500 nelli, A. Sips, M. Stamp, and S. Wiesen, “Impact of nitrogen seeding on confinement and  
501 power load control of a high-triangularity JET ELMy H-mode plasma with a metal wall,”  
502 *Nuclear Fusion*, vol. 53, no. 11, p. 113025, 2013.
- 503 [20] P. A. Schneider, L. B. Orte, A. Burckhart, M. G. Dunne, C. Fuchs, A. Gude, B. Kurzan,  
504 W. Suttrop, E. Wolfrum, and the ASDEX Upgrade Team, “Pedestal and edge localized  
505 mode characteristics with different first wall materials and nitrogen seeding in ASDEX  
506 Upgrade,” *Plasma Physics and Controlled Fusion*, vol. 57, no. 1, p. 014029, 2015.
- 507 [21] L. Frassinetti, D. Dodt, M. Beurskens, A. Sirinelli, J. Boom, T. Eich, J. Flanagan,  
508 C. Giroud, M. Jachmich, M. Kempenaars, P. Lomas, G. Maddison, C. Maggi, R. Neu,  
509 I. Nunes, C. Perez von Thun, B. Sieglin, M. Stamp, and J.-E. contributors, “Effect of ni-  
510 trogen seeding on the energy losses and on the time scales of the electron temperature and  
511 density collapse of type-I ELMs in JET with the ITER-like wall,” *Nuclear Fusion*, vol. 55,  
512 no. 2, p. 023007, 2015.
- 513 [22] Joseph Ngatchou-Wandji, “On Testing for the Nullity of Some Skewness Coefficients,” *In-*  
514 *ternational Statistical Review*, vol. 74, no. 1, pp. 47–65, 2006.
- 515 [23] W. D. Johnson and J. D. Gibbons, *Nonparametric Statistical Inference*, 1973, vol. 15, no. 2.
- 516 [24] E.L. Lehmann and J. P. Romano, *Testing Statistical Hypothesis*, 3rd ed. Springer, 2005.
- 517 [25] A. Shabbir, G. Verdoolaege, O. J. W. F. Kardaun, and J.-M. Noterdaeme, “Visualization  
518 of the operational space of edge-localized modes through low-dimensional embedding of  
519 probability distributions,” *Review of Scientific Instruments*, vol. 85, no. 11, p. 11E819,  
520 2014.
- 521 [26] G. Verdoolaege, G. Karagounis, M. Tendler, and G. V. Oost, “Pattern recognition in prob-  
522 ability spaces for visualization and identification of plasma confinement regimes and con-

- 523 finement time scaling,” *Plasma Physics and Controlled Fusion*, vol. 54, no. 12, p. 124006,  
524 2012.
- 525 [27] A. Shabbir, G. Verdoolaege, J. Vega, and A. Murari, “ELM Regime Classification by Con-  
526 formal Prediction on an Information Manifold,” *IEEE Transactions on Plasma Science*, pp.  
527 1–10, 2015.
- 528 [28] A. Loarte, G. Saibene, R. Sartori, D. Campbell, M. Becoulet, L. Horton, T. Eich, A. Her-  
529 rmann, G. Matthews, N. Asakura, A. Chankin, A. Leonard, G. Porter, G. Federici, G. Janes-  
530 chitz, M. Shimada, and M. Sugihara, “Characteristics of type I ELM energy and particle  
531 losses in existing devices and their extrapolation to ITER,” *Plasma Physics and Controlled  
532 Fusion*, vol. 45, no. 9, pp. 1549–1569, 2003.
- 533 [29] A. Loarte, M. Becoulet, G. Saibene, R. Sartori, D. J. Campbell, T. Eich, A. Herrmann,  
534 M. Laux, W. Suttrop, B. Alper, P. J. Lomas, G. Matthews, S. Jachmich, J. Ongena,  
535 P. Innocente, and EFDA-JET Workprogramme Collaborators, “Characteristics and scaling  
536 of energy and particle losses during Type I ELMs in JET H-modes,” *Plasma Physics and  
537 Controlled Fusion*, vol. 44, no. 9, pp. 1815–1844, sep 2002.
- 538 [30] P. B. Snyder, H. R. Wilson, J. R. Ferron, L. L. Lao, A. W. Leonard, T. H. Osborne, A. D.  
539 Turnbull, D. Mossessian, M. Murakami, and X. Q. Xu, “Edge localized modes and the  
540 pedestal: A model based on coupled peelingballooning modes,” *Physics of Plasmas*, vol. 9,  
541 no. 5, p. 2037, 2002.
- 542 [31] N. Oyama, Y. Sakamoto, A. Isayama, M. Takechi, P. Gohil, L. Lao, P. Snyder, T. Fu-  
543 jita, S. Ide, Y. Kamada, Y. Miura, T. Oikawa, T. Suzuki, H. Takenaga, K. Toi, and the  
544 JT-60 Team, “Energy loss for grassy ELMs and effects of plasma rotation on the ELM  
545 characteristics in JT-60U,” *Nuclear Fusion*, vol. 45, no. 8, pp. 871–881, 2005.
- 546 [32] T. Osborne, J. Ferron, R. Groebner, L.L.Lao, A.W.Leonard, M. Mahdavi, R.Maingi,  
547 R. Miller, A. Turnbull, M.Wade, and J.Watkins, “The effect of plasma shape on H-mode  
548 pedestal characteristics on DIII-D,” *Plasma Physics and Controlled Fusion*, vol. 42, no.  
549 Supplement 5A, pp. A175–A184, 2000.
- 550 [33] H.Zohm, *Magnetohydrodynamic Stability of Tokamaks*. Wiley-Vch, 2015.